

## Advanced laser speckle techniques characterize the complex thermomechanical properties of thin multilayered structures

Peter Zimprich<sup>a</sup> and Bernhard G. Zagar<sup>b</sup>

<sup>a</sup> Faculty for Physics, Physics of Nanostructured Materials, University of Vienna, Dr. Karl-Lueger Ring 1, A-1010 Vienna, Austria; peter.zimprich@univie.ac.at

<sup>b</sup> Institute for Measurement Technology, University of Linz, Altenberger Str. 69, A-4040 Linz, Austria

Received 13 November 2007

**Abstract.** Non-contacting methods for strain and displacement measurement are now well established, although not widely used in material science. Some applications like the determination of coefficients of thermal expansion, especially of thin multilayered structures, are particularly demanding and definitely require non-contacting methods. The paper shows that laser speckle pattern shift techniques can be successfully utilized for that kind of strain and displacement measurements. We elaborate a theory of laser speckle displacement estimation and show that these optical systems are sufficiently rigid and sensitive to determine the values of thermal expansion coefficients for small to medium-sized Si-based semiconductor devices like insulated gate bipolar power transistors.

**Key words:** thermal expansion coefficient, laser speckle technique, multilayered structures.

### 1. INTRODUCTION

The optical principle, governing the laser speckle pattern shift technique to determine strain, was originally devised by Yamaguchi [1] and later improved by several authors [2–5]. Their main goal was to improve the general applicability of this technique and to advance the strain resolution by improving the digital signal processing, eliminating the effects of the rigid body motions and rotations of the specimen. These rigid body motions and rotations are always present in practical loading situations [6].

Several authors [7,8] have discussed various aspects of laser-based systems in general, considering holographic [9] and moiré [4] methods, laser-interferometry [10] and laser speckle interferometry [4,9] and have shown that most of them are more sensitive to the above-mentioned rigid body displacements than the laser speckle shift method, discussed in this paper.

The paper is organized as follows. The optical principle, governing the system, is explained first; secondly the digital signal processing of speckle images and their load-dependent structural changes are discussed, which is necessary to achieve high strain resolution. Thirdly, the system's application to thermal strain measurement in highly structured medium-size semiconductors is considered.

## 2. OPTICAL PRINCIPLE

Laser speckles is a phenomenon that is experienced if an optically rough surface is illuminated by a highly coherent laser source. They are formed by the interference of dephased but coherent wavelets, emanating from different microscopic elements of the specimen's surface and cause a randomly looking pattern, an example of which is shown in Fig. 1.

This speckle pattern is characteristic for a particular surface element just like a fingerprint and if that surface element is undergoing a pure displacement  $\Delta_{\text{surf}}$ , the associated speckles, as recorded by a camera at a fixed location, are displaced likewise by  $\Delta_{\text{image}}$  as is shown in Fig. 2.

If the specimen, in addition to pure displacement, is also strained, the associated structural changes of the speckles will for most applications cause a negligible additional speckle-displacement [5,11-13]. The usual digital image-processing algorithm, used to track speckles, is based on pattern matching by some kind of

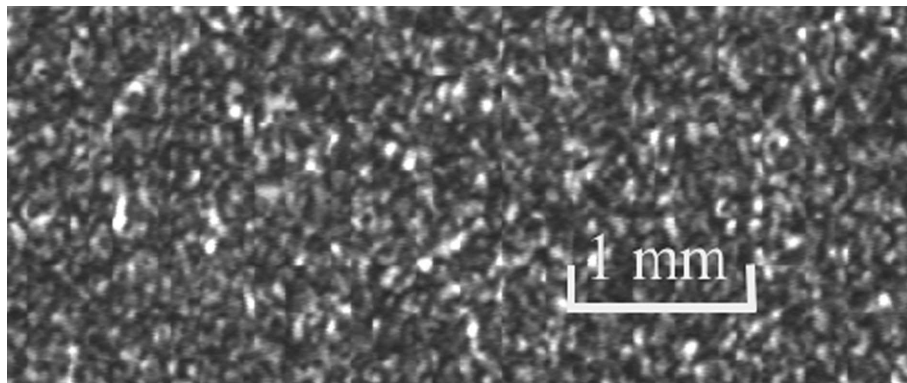


**Fig. 1.** Typical objective speckle image as recorded by an area-scan camera, placed at a distance of 135 mm from a laser illuminated rough aluminium specimen.

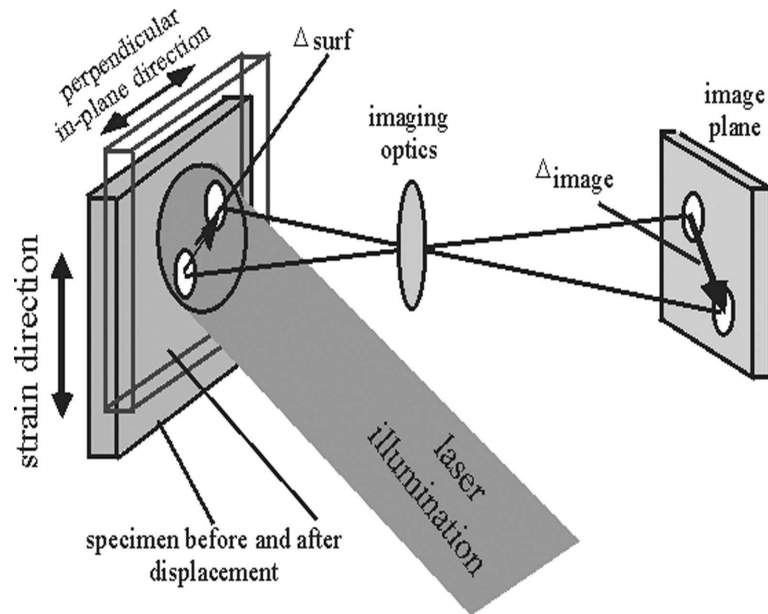


**Fig. 2.** Basic optical set-up for the tracking of laser speckles caused by the displacement of elements of the specimens surface.

correlation algorithm, which usually gives displacement values that are integer multiples of a quant (usually the size of the pixel pitch of the camera).

Since often in material science applications one is interested only in one-dimensional strain measurement, the optical set-up of Fig. 2 can be reduced to be sensitive only in one dimension by applying Fourier-optical filtering [5,12] and using a line-scan camera instead of an area-scan camera. The following discussion assumes one-dimensional signals.

### 3. SIGNAL PROCESSING

Consider the model of initial (unloaded)  $I(x, y)$  and displaced (under load)  $I(x - D, y)$  laser speckle intensities ( $D$  is the speckle displacement at the faceplate of the camera) as projected onto a suitable line-scan camera, which serves as a discretization unit by averaging over its finite pixel aperture, spaced on a regular pixel pitch:

$$\begin{aligned} x_0(i) &= s_0(i) + n_0(i), \\ x_d(i) &= s_d(i) + n_d(i), \end{aligned} \quad (1)$$

where  $n_0(i)$  and  $n_d(i)$  are mutually uncorrelated noise signals that are also uncorrelated with the signals  $s_0(i)$  and  $s_d(i)$  that are displaced versions of each other:

$$\begin{aligned}
s_0(i) &= \int_{i \cdot p - w/2}^{i \cdot p + w/2} \int_{-h/2}^{+h/2} I(x, y) \, dx \, dy, \\
s_d(i) &= \int_{i \cdot p - w/2}^{i \cdot p + w/2} \int_{-h/2}^{+h/2} I(x - D, y) \, dx \, dy.
\end{aligned} \tag{2}$$

Here  $i$  is the pixel index,  $p$  is the pixel pitch ( $p = 7 \mu\text{m}$  typically for a line-scan camera),  $w$  is the width of a pixel ( $w = 5.5 \mu\text{m}$ ), and  $h$  is the height of a pixel ( $h = 7 \mu\text{m}$ ). It can be shown [11] that the correlation function  $R$ , which depends on the parameter  $\tau$

$$R_{x_0, x_d}(\tau) = E \{x_0(i) \cdot x_d(i)\} = R_{s, s}(\tau - D), \tag{3}$$

has a peak at the displacement value  $D$ , if the so-called fill factor of the camera is equal to unity. This means that the effective width  $w$  of each pixel approaches the pixel pitch  $p$ .

Since, different from Eq. (3), we are considering discrete data, the peak of the correlation function will also occur at an integer multiple  $k$  of the pixel pitch  $p$  even though the displacement value  $D$  is clearly a continuous variable. Driven by the desire to achieve as high a resolution of the displacement value  $D$  as possible and also to save on computational complexity as much as possible to keep the measuring rate high, one would like to overcome the problem of CPU-time intensive sub-pixel interpolation. A way to achieve this is to estimate the displacement using phase information as shown in [11] and to modify it as shown below.

As shown in Eq. (3), the cross-correlation function  $R_{x_0, x_d}$ , calculated from the two signals  $x_0(i)$  and  $x_d(i)$  under the assumption that the noise terms are uncorrelated (statistically independent), is given by a displaced (displacement value  $D$ ) version of the autocorrelation function of the signal component alone,  $R_{s, s}(\tau - D)$ , as is shown in Fig. 3.

Performing the displacement calculation in the frequency domain by applying the Fourier transform to Eq. (3) yields

$$\begin{aligned}
P_{x_0, x_d}(f) &= P_{s_0, s_d}(f) = 2 \int_{-\infty}^{+\infty} R_{s, s}(\tau) e^{-j2\pi f \tau} \, d\tau \\
&= P_{s, s}(f) e^{-j2\pi f D},
\end{aligned} \tag{4}$$

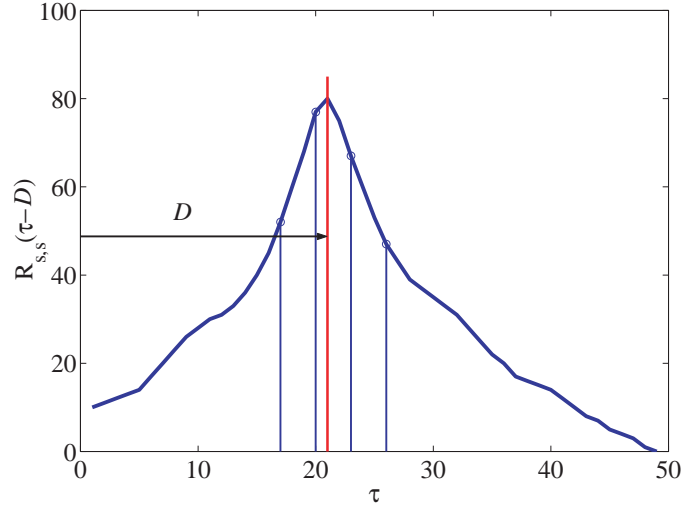


**Fig. 3.** Cross-correlation function estimate as a displaced (parameter  $D$ ) version of the auto-correlation function of the signal component.

where  $P_{s,s}(f)$  is the spectral density of the deterministic power component (the speckle intensity pattern) and  $P_{x_0,x_d}(f)$  is the cross-spectral density of the imaged intensity signals (speckles plus noise) before and after the displacement. The displacement appears in the cross spectrum as a phase function  $\phi(f)$ , which in the case of a non-dispersive transfer function is a linear function of the discrete frequency index  $m$  as shown in Fig. 4 for some experimental data.

Discrete version of Eq. (4) can be written as

$$\begin{aligned}
 P_{s_0,s_d} \left( \frac{2\pi}{N} m \right) &= \frac{2}{\Delta X n_d} \sum_{j=1}^{n_d} F_{s_0}^j \left( \frac{2\pi}{N} m \right) F_{s_d}^{j*} \left( \frac{2\pi}{N} m \right) \\
 \phi \left( \frac{2\pi}{N} m \right) &= \arctan \left\{ \frac{\Im \{ P_{s_0,s_d}(\frac{2\pi}{N} m) \}}{\Re \{ P_{s_0,s_d}(\frac{2\pi}{N} m) \}} \right\}, \quad (5)
 \end{aligned}$$

where

$$F_{s_0}^j \left( \frac{2\pi}{N} m \right) = \sum_{k=0}^{N-1} s_0((j-1)N + k) e^{-j \frac{2\pi}{N} km}$$

is the Fourier transform of the signal  $s_0$ ,  $\Delta X = \Delta x N$  is the discrete data segment length,  $n_d$  is number of segments of the length  $\Delta x$ ,  $X = n_d \Delta X$  is the total length of speckle data,  $j$  is the index, selecting one subsegment and  $\Delta x$  is the pixel pitch, scaled by the magnification of the imaging optics.

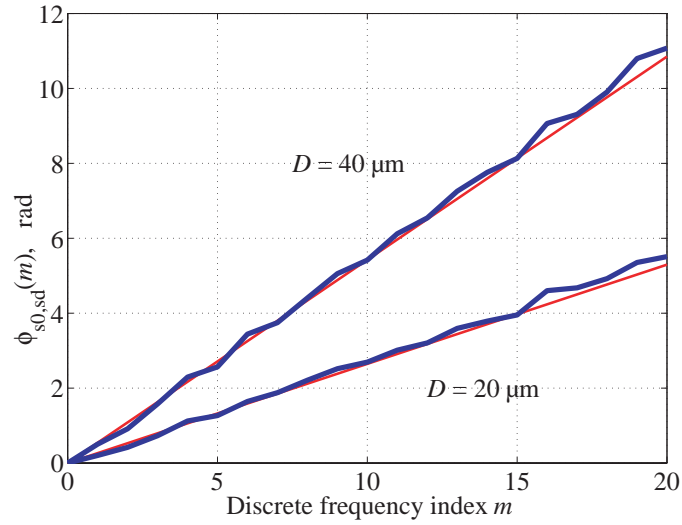


**Fig. 4.** Phase argument of the cross spectrum of initial and displaced speckle images for two different values of the displacement parameter  $D$  with regression lines indicated. The deviation at higher frequencies is assumed to be caused by displacement-dependent structural changes in the speckle patterns that express themselves in higher frequency components.

As can be seen from Fig. 4, the phase as calculated through Eq. (5) differs considerably from a linear phase function; thus it is interesting to quantify the achievable variance or precision of the phase estimator.

From [11] it is known that the standard deviation  $\sigma$  of the phase data can be approximated by

$$\sigma \left[ \hat{\phi}_{s_0, s_d} \left( \frac{2\pi}{N} m \right) \right] \approx \arcsin \left\{ \frac{1 - C_{s_0, s_d} \left( \frac{2\pi}{N} m \right)}{2C_{s_0, s_d} \left( \frac{2\pi}{N} m \right)} \right\}, \quad (6)$$

where  $m = 1, 2, \dots, \frac{N}{2}$  (index of the discrete frequency component),  $C_{s_0, s_d}(\dots)$  is the coherence function of signals  $s_0$  and  $s_d$  at frequency  $2\pi m/N$  and  $\sigma[\dots]$  is standard deviation.

The coherency function  $C_{s_0, s_d}(f)$  is defined as

$$C_{s_0, s_d}(f) = \frac{|P_{x_0, x_d}(f)|^2}{P_{x_0, x_0}(f)P_{x_d, x_d}(f)}. \quad (7)$$

It is a measure of spectral correlation, considered for the frequency component centered at  $f$ .

Since it is known that  $\phi_{s0,sd}(0) = 0$ , the minimum error estimate of the slope  $b$  of the regression lines (Fig. 4), which determine the measured displacement, can be estimated (denoted by  $\hat{b}$ ) to be:

$$\hat{b} = \frac{\sum_{m=1}^{N/2} \left(\frac{2\pi}{N}m\right) \phi_{s0,sd}\left(\frac{2\pi}{N}m\right)}{\sum_{m=1}^{N/2} \left(\frac{2\pi}{N}m\right)^2}. \quad (8)$$

The variance of the slope is approximately given by [11]:

$$\sigma^2[\hat{b}] \cong \frac{1}{\sum_{m=1}^{N/2} \frac{\left(\frac{2\pi}{N}m\right)^2}{\sigma^2\{\phi_{s0,sd}\left(\frac{2\pi}{N}m\right)\}}}, \quad (9)$$

from which the estimate of the displacement  $\hat{D}$  and the standard deviation of the displacement  $\sigma[\hat{D}]$  can be easily calculated:

$$\hat{D} = \frac{1}{2\pi} \frac{\sum_{m=1}^{N/2} f_m \phi_{s0,sd}(m)}{\sum_{m=1}^{N/2} f_m^2}, \quad (10)$$

$$\sigma[\hat{D}] = \frac{1}{8\pi n_d \sum_{m=1}^{N/2} \frac{f_m^2 C_{s0,sd}(f_m)}{1 - C_{s0,sd}(f_m)}}, \quad (11)$$

where  $f_m = \frac{m}{\Delta x N}$  is the spatial frequency for index  $m$ .

As is shown by Piersol [11], Eq. (10) is equivalent to the Cramér–Rao lower bound [14] on the variance of the (unbiased) displacement estimation error and hence the phase-based displacement estimator is optimal in that sense since it attains the bound. Using typical noise figures of cameras and considering typical 8-bit discretizations, the standard deviation of the displacement estimator  $\hat{D}$  will be of the order of 0.1  $\mu\text{m}$ . This estimation does neither include instabilities of the laser source nor any mechanical vibrations of the loaded specimen.

### 3.1. The implemented algorithm

An algorithm, based on Eqs. (5) and (10), was coded in C and run in a real-time Linux environment. The following processing steps are performed in real-time for each signal, recorded by the line-scan camera.

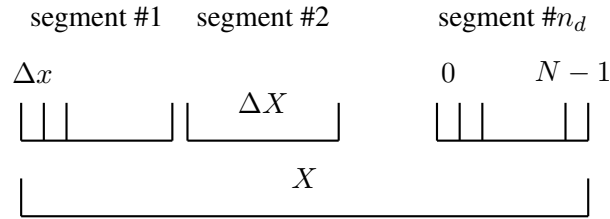


**Fig. 5.** Definitions of the parameters of Eq. (5).

- Acquisition of the pixel values within a section of interest of the camera (Fig. 5).
- Segmentation of the data into  $n_d$  intervals of  $N$  samples each.
- Removal of the segment mean in each segment.
- Application of a data window in each segment in order to reduce the effects of sidelobes and to decrease the estimation bias.
- Calculation of the discrete Fourier transform.
- Calculation of the phase through Eq. (5) using the computed Fourier transform  $F_{s0}^j(\dots)$  of the reference data.
- Estimation of the displacement  $\hat{D}$ , calculated by a weighted version of Eq. (10), which takes into account that only those spectral lines with coherence values close to one show good spectral correlation.

For a total of 3000 pixels, segmented into  $n_d = 12$  non-overlapping segments, the calculation time on a Pentium class PC (800 MHz) was determined to be significantly less than 10 ms.

#### 4. THE THERMAL MISMATCH PROBLEM IN INSULATED GATE BIPOLAR TRANSISTOR (IGBT) TECHNOLOGY

The presented laser speckle technique is a powerful tool for high-resolution strain measurements compared to classical techniques (e.g. strain or clip gauges), especially in cases of very small or thin samples, where no surface marking or surface preparation is possible or could affect adversely the results. Because of these unique advantages of laser speckle methods, these can be applied to a problem of high interest in the electronics industry known as the “thermal mismatch problem”. It is one of the most important issues in quality and reliability management of electronic devices. To employ it, a laser speckle sensor was combined with a furnace (called Laser Speckle Dilatometer LSBD) to measure thermal strains and thermal expansion coefficients of thin metallization layers. Modern electronics and power electronics consist of a variety of different thin materials with pronounced differences in thermal expansion coefficients stacked

in closed packed multilayered structures. During operation these electronic devices are exposed to cyclic thermal loading and thus high thermal stresses can develop in the layered material. This can possibly degrade the device by initiating crack development or delamination, leading to catastrophic failure of the device. Knowledge of the thermal expansion behaviour is also a crucial part of the finite element based design rules and reliability estimates as pointed out in this chapter.

Power semiconductor modules with semiconductor based IGBTs (Fig. 6) are very convenient devices for controlling current and frequency in high power applications; thus the application of power devices like IGBTs and diodes has dramatically increased for industrial applications in the last decade [15].

These power devices are vertically oriented components. That is, the current flows vertically through the device. Due to the development of new generations of chips, the size and the thickness of silicon base material is reduced, which has a great influence on the electrical parameters like power losses. For the minimization of power losses and switching parameters, the thickness of the devices is reduced by every new chip generation and will be further reduced in the future. Typical thickness of today's power chips is from 70  $\mu\text{m}$  up to some hundreds of micrometers. On both sides of the device, metallizations are deposited on the surface. This "sandwich" of metal–Si–metal is a combination of different materials and therefore of different coefficients of thermal expansion (CTEs).

By the reduction of the thickness of the Si semiconductor material with respect to the metal layer, the influence of the metals on both sides increases and becomes a more dominant factor. Today the typical joining techniques used for power devices

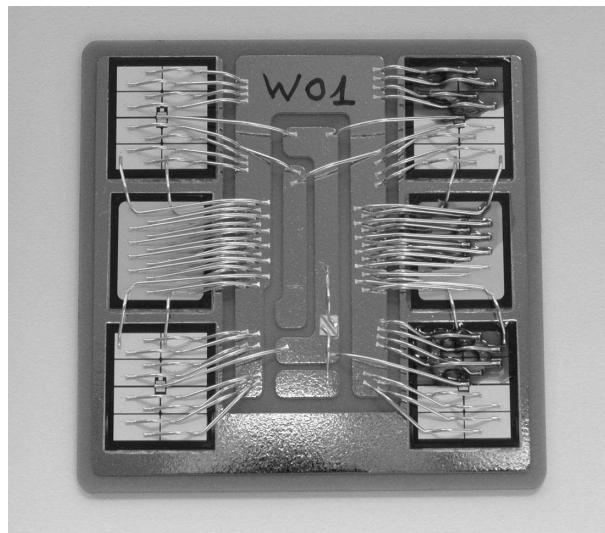


**Fig. 6.** Microphotograph of an insulated gate bipolar transistor IGBT. Shown is a typical chip-configuration. The actual chip size is approximately  $10 \times 10 \text{ mm}^2$ .

are heavy wire bonding on the top side and soldering on the bottom side. The reliability of these joining techniques are always influenced by the differences in the CTE (thermal mismatch) between the connected partners, which lead to thermal stresses, ultimately leading to crack initiation and propagation during normal operation [16,17].

As the knowledge of the exact value of the CTE for a “final” power chip (metal–Si–metal) is very important for the interpretation and simulation of reliability test results, a technique is needed for giving the opportunity to determine the “effective” CTE values of thin metallization layers on thick substrates, necessary to calibrate simulation models and to verify the influence on reliability testing. In manufacturing of IGBTs, the knowledge of the thermal behaviour of metallized substrates plays an important role for a reliable design. Because of the large differences of CTEs between the materials involved (e.g. 24 ppm/°C for Al, 2–3 ppm/°C for Si), their influence on the thermal expansion behaviour of Si with a thin metallization layer of Al is of a particular importance [18,19].

#### **4.1. Thermal calibration of the LSBD**

Calibration tests, determining the CTE of the Copper Standard Reference Material NIST SRM 736 (a rod material with 6 mm diameter) showed high accuracy and reliability of the measured strain values. Successive runs show high reproducibility (1.5%) of CTEs and very good agreement with the reference data. Up to 250 °C the deviation of the measured thermal strain values is lower than 7% compared to the mentioned reference material. The strain resolution depends on the speckle tracking accuracy and the baselength, over which the displacement is integrated; it was determined to be of the order of  $2 \times 10^{-5}$ .

#### **4.2. The laser speckle dilatometer (LSBD)**

Our samples were heated up from room temperature to maximum 150°C and the temperature of the specimen was determined within an error margin of  $\pm 0.5^\circ\text{C}$ . The heating rate was set to be less than 1 deg/min. The heating chamber (Fig. 7) was designed also for low-temperature measurements until about  $-100^\circ\text{C}$  using a liquid nitrogen temperature buffer, which can be adjusted to achieve different rates for heating up the samples. The sample chamber can be flooded with argon gas to avoid surface oxidation of the samples, which is especially important beyond 200°C. With the set-up, schematically shown in Fig. 8, and tracking continuously two spots on the specimen’s surface (separated by the baselength  $b$ ), thermal strain data of thin multilayered structures can be measured with a reproducibility of 1.5% between different runs on one sample. For typical measurements three successive runs were performed (Fig. 9). Measurements of thermal expansion of a thin Al metallization layer of 3  $\mu\text{m}$  thickness were carried out on Si substrates with 300  $\mu\text{m}$  thickness for different industrial chips, which were prepared from the commercial modules after removing the bonding wires.

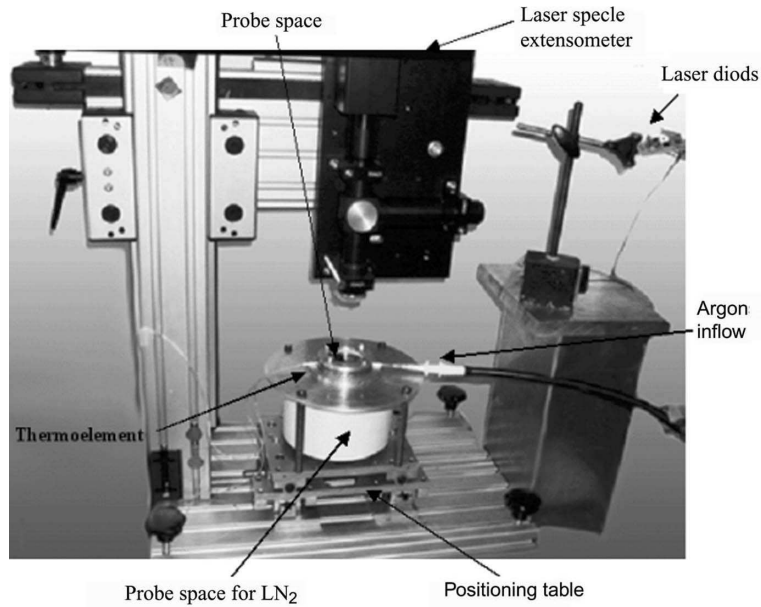


**Fig. 7.** Practical realization of the laser speckle dilatometer. One can see the heating stage at the base below the laser speckle system viewing downward.

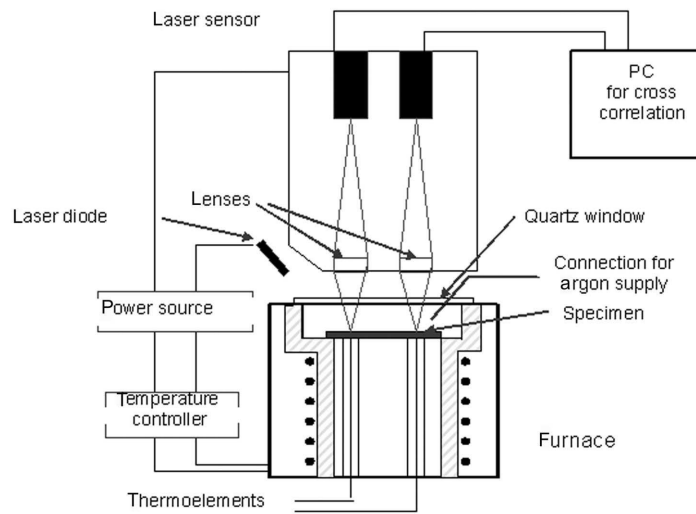


**Fig. 8.** Thermal strain measurement set-up. It consists of two laser sources, illuminating two distinct spots on the specimen's surface (separated by a distance  $D$ ) whose displacements ( $\Delta D_i$ ;  $i = 1, 2$ ) are continuously tracked to derive strain values.

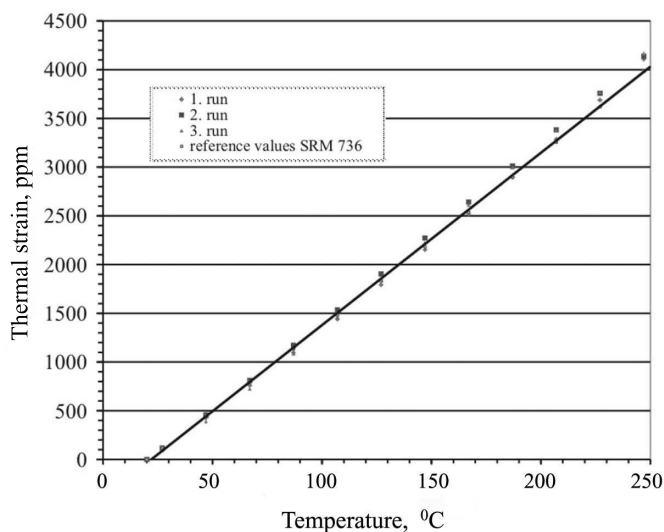


**Fig. 9.** Thermal expansion of NIST Copper SRM 736 (black dots) for three successive runs with the laser speckle dilatometer.

## 5. RESULTS

With the presented LSBD set-up it could be shown, that for a thick ( $300\ \mu\text{m}$ ) Si substrate, the  $3\ \mu\text{m}$  aluminium layer was clearly impeded in CTE down to about  $12\ \text{ppm}/^\circ\text{C}$ , compared to the bulk value of  $24\ \text{ppm}/^\circ\text{C}$  (Fig. 10). It can be assumed, that the thick substrate restricts the thin layer in its thermal expansion because of higher stiffness and therefore more pronounced mechanical constraint effects lead to a reduced CTE value on the aluminium surface [20,21]. From the theory of multilayered structures it can be shown that the influence of a thin layer deposited on a thick substrate will become important for layer thickness of about 8% of the substrate thickness [22]. This has interesting implications for the understanding of thermally driven processes during fabrication of these layers and also for the simulation of multilayer behaviour.

## 6. CONCLUSIONS

A new laser speckle based dilatometer, originally designed for strain measurements of freestanding thin films and fibres, was successfully applied for non-contacting CTE measurements of thin metallic layers on relatively thick and brittle substrates. The non-contacting strain sensor, based on the laser speckle correlation technique, is due to the simple optical arrangement easily adaptable to a temperature chamber and characterized by a high strain resolution of the order

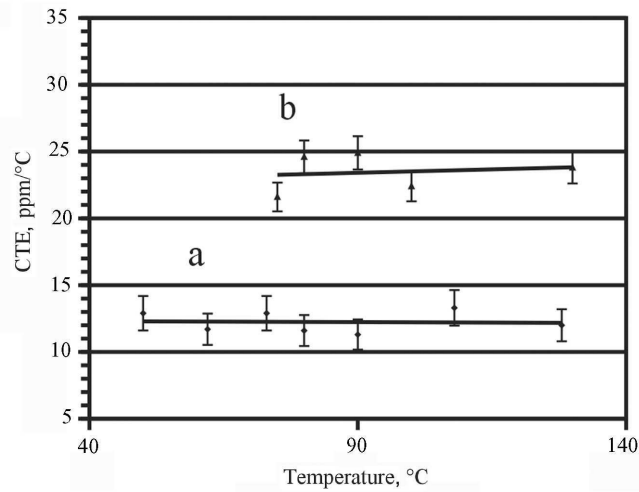


**Fig. 10.** CTE behaviour of a 3  $\mu\text{m}$  Al layer on a 300  $\mu\text{m}$  Si-chip substrate (a); for comparison the measured bulk CTE of Al is indicated (b).

of  $2 \times 10^{-5}$ . This method achieves sufficient degree of accuracy and precision for CTE evaluation in the temperature range from  $-100^\circ\text{C}$  up to  $300^\circ\text{C}$ . Various applications in material science like CTE evaluation of metals, polymers, ceramic components and multilayer structures can be distinguished that require techniques, allowing to avoid any kind of surface preparation. With this system it could be shown that the thermal expansion behaviour of metallization layers is significantly influenced by the thickness of the substrate, resulting in a clear reduction of CTE values of the aluminium metallization layer (“effective CTE”). The knowledge of these true thermal expansion values is crucial for processes like ultrasonic bonding and the estimation of joint reliability. With this new method it seems to be possible to improve the understanding and simulation of thermal mismatch problems in multilayered structures, especially in the case of thin metallization films and printed circuit boards.

## REFERENCES

1. Yamaguchi, I. A laser-speckle strain gauge. *J. Phys. E: Sci. Instrum.*, 1981, **14**, 1270–1273.
2. Sjö Dahl, M. A whole field speckle strain sensor. In *Proc. SPIE Conference on Optical Engineering*. Yokohama, 1999.
3. Tuma, M. L. Results from real-time laser speckle-shift strain measurements. *Opt. Eng.*, 2000, **39**, 498–504.
4. Kobayashi, A. S. (ed.). *Handbook of Experimental Mechanics*. Society for Experimental Mechanics, VCH, New York, 1993.

5. Goodman, J. W. *Introduction to Fourier Optics*. McGraw-Hill, New York, 1968.
6. Anwander, M., Zagar, B. G., Weiss, B. and Weiss, H. Noncontacting strain measurements at high temperatures by the digital laser speckle technique. *Exp. Mech.*, 2000, **40**, 697–702.
7. Schneider, S. C., Rupitsch, S. J. and Zagar, B. G. Signal processing for laser speckle strain measurement techniques. *IEEE Trans. Instr. Measur.*, 2007, **56**, No. 6.
8. Kargel, C. and Zagar, B. G. Optimum analog to digital converters for a laser speckle correlation based displacement and strain sensor with optical preprocessing. *Opt. Eng.*, 2001, **40**, 90–94.
9. Jones, R. and Wykes, C. *Holographic and Speckle Interferometry*, 2nd ed. Cambridge Univ. Press, 1989.
10. Sharpe, W. N., Jr. Development and application of an interferometric system for measuring crack displacements. Final Report, NASA-CR-145106, 77N12367, 1977.
11. Piersol, A. G. Time delay estimation using phase data. *IEEE Trans. Acoust. Speech Signal Process.*, 1981, **29**, 471–477.
12. Zagar, B. G. and Kargel, C. A laser-based strain sensor with optical preprocessing. *IEEE Trans. Instr. Measur.*, 1999, **48**, 97–101.
13. Schneider, S. *Entwicklung eines laser-optischen Messsystems zur berührungslosen Bestimmung von mechanischen Materialparametern*. Ph.D Thesis. University of Linz, 2005.
14. Kay, S. *Fundamentals of Statistical Signal Processing – Estimation Theory*. Prentice Hall, Englewood Cliffs, 1998.
15. Lefranc, G., Weiss, B., Klos, C., Dick, J., Khatibi, G. and Berg, H. Aluminium bond-wire properties after 1 billion mechanical cycles. *Microelectronics Reliab.*, 2003, **43**, 1833–1838.
16. Berg, H. and Wolfgang, E. Advanced IGBT modules for railway traction testing for thermal fatigue effects due to traction cycles. *Microelectronics Reliab.*, 1998, **38**, 1353–1359.
17. Ramming, S., Türkes, P. and Wachutka, G. Crack mechanism in wire bonding joints. *Microelectronics Reliab.*, 1998, **38**, 1301–1305.
18. Ziebs, J., Bresers, J., Frenz, H., Hayhurst, D. R., Klingelhöffer, H. and Forest, S. In *Proc. Intl. Symposium on Local Strain and Temperature Measurement in Non-uniform Fields at Elevated Temperatures*. Woodhead, Cambridge, UK, 1996.
19. Zimprich, P., Licht, T. and Weiss, B. A new method to characterize the thermomechanical response of multilayered structures in power electronics. *Microelectronics Reliab.*, 2006, **46**, 1844–1847.
20. Zoo, Y., Adams, D., Mayer, J. W. and Alford, T. L. Investigation of the coefficient of thermal expansion of silver thin film on different substrates using X-ray diffraction. *Thin Solid Films*, 2006, No. 513, 170–174.
21. Fang, W. and Lo, Ch.-Y. On the thermal expansion coefficients of thin films. *Sensors Actuators*, 2000, **84**, 310–314.
22. Brezina, S. *Anwendung eines Laserinterferometers zur berührungslosen Messung der lokalen Wärmeausdehnung von verschiedenen Materialien*. Dipl. Thesis, University of Vienna, 1996.

## **Lasertäpp-tehnoloogia arendused õhukeste paljukihiliste struktuuride komplekssete termomehaaniliste omaduste iseloomustamiseks**

Peter Zimprich ja Bernhard G. Zagar

Kontaktivabad meetodid mehaaniliste pinge ja objekti asendi mõõtmiseks on tuntud, kuid mitte veel laialdaselt kasutusel. Näiteks võiks olla õhukeste paljukihiliste struktuuride soojuspaisumise teguri määramine. Artiklis on näidatud, et sellisel juhul saab edukalt kasutada lasertäpi kujutise nihkumise tehnikat. Autorite poolt välja töötatud teooria ja eksperimendid näitavad, et selline optiline tehnika võimaldab küllaldase täpsusega määrata soojuspaisumise tegureid väikeste ja keskmise suurusega Si-pooljuhtseadistes, näiteks isoleeritud paisuga bipolaarsetes võimsustransistorites.